

# Ionization–excitation of helium to $\text{He}^+(2p)$ magnetic sublevels following electron, proton, and molecular hydrogen ( $\text{H}_2^+$ and $\text{H}_3^+$ ) impact

H Merabet<sup>1</sup>, R Bruch<sup>1</sup>, S Fülling<sup>1</sup>, K Bartschat<sup>2</sup> and A L Godunov<sup>3</sup>

<sup>1</sup> Department of Physics, University of Nevada Reno, Reno, NV 89557, USA

<sup>2</sup> Department of Physics and Astronomy, Drake University, Des Moines, IA 50311, USA

<sup>3</sup> Department of Physics, Old Dominion University, Norfolk, VA 23459, USA

Received 7 May 2003

Published 23 July 2003

Online at [stacks.iop.org/JPhysB/36/3383](http://stacks.iop.org/JPhysB/36/3383)

## Abstract

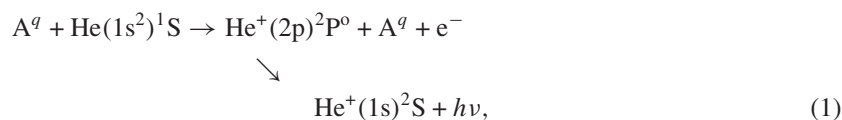
Experimental magnetic sublevel scattering-angle-integrated cross sections following ionization–excitation of  $\text{He}(1s^2)^1\text{S}$  to  $\text{He}^+(2p)^2\text{P}^o$  in  $e^- + \text{He}$  and  $\text{H}_m^+ + \text{He}$  ( $m = 1-3$ ) collision systems have been determined using a combination of total cross sections and polarization fraction measurements in the extreme ultraviolet range. The derived magnetic sublevel cross sections,  $\sigma_0$  and  $\sigma_1$ , for  $M_L = 0 \pm 1$  have been studied over a wide range of velocities (2–8.5 au) for electron impact on helium. These results are compared with previous experimental proton cross sections (2–6 au) as well as new measured data for hydrogen molecular impact (1.4–4.0 au) for equi-velocity. In addition, our electron and proton measurements are compared with earlier theoretical predictions, our recent second-Born calculations fully including off-shell energy terms, and present predictions from a hybrid first-order and second-order distorted-wave plus  $R$ -matrix (close-coupling) model (DWB1 + RMPS and DWB2 + RMPS). Finally, we have extended our polarization measurements for  $\text{H}^+ + \text{He}$  collisions and found excellent agreement between theory and experiment at nearly all impact energies. However, the present second-Born and DWB1 + RMPS results deviate slightly from the experimental electron data while the DWB2 + RMPS calculations tend toward the experimental data of Forand *et al* (1985 *J. Phys. B: At. Mol. Phys.* **18** 1409).

## 1. Introduction

There is at present a considerable interest in few-electron processes induced by intermediate to high-energy charged particle impact on atomic and molecular targets (McGuire 1997, Bruch *et al* 1993) such as double ionization, double excitation (Bruch *et al* 2002), and ionization–excitation. These many-body aspects of atomic collision processes are associated with electron–electron correlations and other few-body dynamical phenomena that supersede

independent-particle models (Niehaus 1986). Most experiments have focused on two-electron processes in helium, since this is the simplest target containing more than one electron, and it is therefore ideally suited to achieving a better theoretical understanding of the few-body problem (Merabet *et al* 2002b, Godunov *et al* 2001, Fang and Bartschat 2001a, Rouvellou *et al* 2000, Balashov and Bodrenko 1999, Hayes and Williams 1996) that is likely to be useful for the description of other complex systems, e.g. the dynamic behaviour of atoms in molecules.

When a negatively or positively charged projectile collides with a helium atom at intermediate to high impact energies, the dominant collision mechanisms are elastic scattering, excitation, and ionization of the target with subsequent emission of photons and/or electrons (Fülling *et al* 1992, Bailey *et al* 1995, Stolte and Bruch 1996). Simultaneous ionization–excitation of the target can also occur at sufficiently high energies, but it leads to relatively small emission cross sections (Bailey *et al* 1995), thereby making this process very difficult to observe experimentally. Such a collision can produce the singly ionized  $\text{He}^+(2p)^2\text{P}$  state (also denoted as  $\text{He II}(2p)^2\text{P}$ ) in the case of helium and gives rise to the emission of Lyman- $\alpha$  radiation with a wavelength of 30.4 nm as follows:



where  $\text{A}^q$  could be a negatively or positively charged projectile ( $e^-$ ,  $\text{H}^+$ ,  $\text{H}_2^+$ , or  $\text{H}_3^+$ ).

Until recently, not much work has been done on excitation–ionization of helium by proton and/or molecular hydrogen ( $\text{H}_2^+$  and  $\text{H}_3^+$ ) impact. On the other hand, electron impact on helium has been thoroughly investigated both experimentally and theoretically (Merabet *et al* (2002b) and references therein), because the relatively simple atomic structure of helium makes it a preferred candidate for very stringent comparisons with calculations. The first electron-impact measurement of the polarization of  $\text{He}^+$  radiation emitted in the simultaneous excitation–ionization process was made by Haidt and Kleinpoppen (1966), who studied the  $n = 4 \rightarrow 3$  transition at 468.6 nm. More recent electron measurements are summarized by Heddle and Gallagher (1989). The only visible ultraviolet (VUV) polarization data reported previously were by McConkey *et al* (1988) for the  $n = 4 \rightarrow 2$  transition. An angular distribution of the  $\text{He}^+(2p)^2\text{P}^0$  alignment induced by electron impact was reported by Götz *et al* (1996). The first polarization measurements of He II Lyman- $\alpha$  and Lyman- $\beta$  were performed by Merabet *et al* (1999, 2001a).

Most previous ionization–excitation studies yielded total, doubly, or triply differential cross sections only and did not give any information about the population of magnetic sublevel cross sections corresponding to  $M_L = \pm 1$  and 0. Furthermore, the observed systematic deviation of experimental data from the predictions obtained in the most sophisticated theoretical calculations presently available raises questions about the validity of the normalization procedures. In particular, there are concerns about the absolute values of  $\text{He II}(2p)^2\text{P}^0$  cross sections derived from undispersed VUV radiation and the filters used to isolate the 30.4 nm wavelength emission from the dominant He I emission ( $\lambda = 58.4$  nm). A summary of previous absolute measurements and their limitations is given by Dogan *et al* (1998). One class of experiments, which are free from such problems, are polarization and angular distribution studies, which make use of relative intensity measurements. Such measurements of the polarization or angular distribution of the photons emitted by excited atoms and ions generate important information pertaining to the magnetic sublevel populations which can be used to test theoretical approaches at a different level than that accessible through angle-integrated or angle-differential cross section measurements.

In this work we have investigated the degree of linear polarization  $P$  of the radiation emitted after electron and positively singly charged ion impact on helium. Because of the cylindrical symmetry of our collision experiment,  $P$  can be defined as

$$P = \frac{I_{\parallel} - I_{\perp}}{I_{\parallel} + I_{\perp}}. \quad (2)$$

Here  $I_{\parallel}$  and  $I_{\perp}$  are the intensities of radiation with electric field vectors parallel and perpendicular with respect to the incident projectile beam direction when measured at an angle of 90°. The degree of linear polarization  $P$  is directly related to the sublevel cross section ratios. Assuming  $LS$ -coupling, where  $L$  and  $S$  are the orbital and spin angular momentum number of the excited levels, the degree of linear polarization for He II(2p)<sup>2</sup>P<sup>o</sup> state can be expressed as (Percival and Seaton 1958):

$$P(^2P^o) = \frac{3(\sigma_0 - \sigma_1)}{7\sigma_0 + 11\sigma_1}, \quad (3)$$

where  $\sigma_{M_L}$  ( $M_L = -1, 0$  and  $1$ ) are the magnetic sublevel angle-integrated excitation cross sections of specific  $M_L$  sublevels ( $\sigma_{-1} = \sigma_1$ ). Moreover, the total cross section  $\sigma$  is the sum of the three magnetic sublevel cross sections,

$$\sigma = \sigma_0 + 2\sigma_1. \quad (4)$$

Thus by combining equation (3) with (4),  $\sigma_{M_L}$  can be obtained for excitation–ionization.

In this work, we have combined measurements of two experimental techniques, namely extreme ultraviolet (EUV) spectrometry and EUV polarimetry, to determine experimental magnetic sublevel cross section results for He II(2p)<sup>2</sup>P<sup>o</sup> excited states following electron, proton, and molecular hydrogen ion (H<sub>2</sub><sup>+</sup> and H<sub>3</sub><sup>+</sup>) impact at a wide range of projectile velocities (1.4–8.5 au). Moreover, a hybrid first-order distorted-wave plus 23-state  $R$ -matrix with pseudo-states (DWB1 + RMPS), as well as advanced second-order approaches such as DWB2 + RMPS and second-Born (Godunov *et al* 2001, Merabet *et al* 2002b) theories are used to predict the polarization fraction and total cross sections for electron and/or proton impact. Finally, all experimental results are compared as function of the projectile velocities in an attempt to elucidate the mechanisms involved in these collision systems.

## 2. Experimental apparatus and cross section determination

Since the experimental set-up has been described in detail by Bailey *et al* (1995, 1999) and Merabet *et al* (1999, 2001a), only a brief discussion is presented here. Positive ion beams (H<sup>+</sup>, H<sub>2</sub><sup>+</sup> and H<sub>3</sub><sup>+</sup>) produced by the University of Nevada Reno 2 MV van de Graaff accelerator and electron beams created by an electron gun deliver projectile beams focused into a differentially pumped target cell. The EUV emission was observed at right angles to the projectile beam and analysed with a 1.5 m grazing incidence monochromator in conjunction with a channeltron detector. For 100 μm slit widths, the monochromator provided a spectral line width (full-width half-maximum: FWHM) of 0.1 nm at  $\lambda = 30.4$  nm, corresponding to a spectral resolution of  $(\lambda/\Delta\lambda) \approx 304$ . The target chamber houses a polarimeter that utilizes a molybdenum–silicon (Mo/Si) multilayer mirror MLM. A PC-controlled data acquisition system is used to operate the apparatus and to record the data. Our polarization measurements have been performed with a 10% VYNS spectral filter (Bailey *et al* 1999, Merabet *et al* 1999) that provides a transmission ratio of He I/He II line intensities of approximately 1:100 000, so that the polarization measured with this filter only contained approximately a 1% contribution from the dominating He I(1snp)<sup>1</sup>P<sup>o</sup> radiative emission. Since sufficiently strong magnetic fields can lead to a depolarization of the observed radiation by the Hanle effect, the gas cell

used in this study was mounted inside a cylindrical magnetic shielding. With this shielding at the interaction region of the gas target a magnetic field smaller than 0.05 G has been achieved. The He II results have been put on the absolute scale by renormalizing our proton data (Merabet *et al* 2002b) to full second-Born cross section values for high velocity impact ( $v = 6.1$  au). The electron (molecular hydrogen) cross sections are then renormalized to protons in a way that keeps electron (molecular hydrogen) to proton cross section ratios the same as those of Bailey *et al* (1995) for equi-velocity projectile impact. In addition, the obtained cross section data have been corrected for alignment effects using (Götz *et al* 1996),

$$\sigma(\theta) = \sigma \times \left\{ 1 + \frac{2P}{P-3} \times P_2(\cos\theta) \right\}, \quad (5)$$

where  $\sigma(\theta)$  is the measured cross section,  $\theta = 90^\circ$  is the observation angle of the emitted photons,  $\sigma$  is the cross section for an isotropic distribution,  $P_2(\cos\theta)$  is the second Legendre polynomial, and  $P$  is the degree of linear polarization. Statistics of the measured line intensities in this study were between 0.5 and 1% over most of the range of impact energies. Since the sum and difference of intensities are involved, the relative error of the polarization fraction increases rapidly with decreasing intensity. The relative error also becomes larger when the polarization fraction is small, reaching a maximum when it is close to zero. When instrument uncertainties related to energy resolution of the van de Graaff accelerator, target pressure stability, polarization, and charge normalization are combined, the total uncertainty for magnetic scattering-angle-integrated sublevel cross sections is found to be about 13–15% for He II(2p)<sup>2</sup>P<sup>o</sup> states. In order to maintain single-collision conditions, a detailed pressure dependence of the emission from ionized-excited helium was investigated with the EUV grazing incidence monochromator and the MLM polarimeter for different projectile impacts. Consequently, a gas pressure of 1 mTorr was adopted for electron impact on helium polarization measurements. For proton impact higher gas pressures were used (about 30 mTorr) since depolarization did not occur for helium pressures less than 40 mTorr. However, for molecular hydrogen projectiles, a pressure of 10 mTorr was employed in order to avoid dissociation of H<sub>2</sub><sup>+</sup> and H<sub>3</sub><sup>+</sup> prior to encountering the emission region of the target cell (Bailey *et al* 1995, Merabet *et al* 2002a). The current He II(2p)<sup>2</sup>P<sup>o</sup> polarization results have not been corrected for cascade effects because the partial magnetic sublevel cross sections for the higher He II ( $n\ell$ ) magnetic substates are not yet accurately known. However, due to the much shorter lifetimes of the excited He II states in comparison with those of He I, cascade effects associated with magnetic sublevel repopulation are expected to be smaller than for He I (Merabet *et al* 2001b).

### 3. Theoretical methods used for e<sup>-</sup> + He collision system

In the present study recent first-order distorted-wave plus 23-state  $R$ -matrix (DWB1 + RMPS) and advanced second-order DWB2 + RMPS methods are utilized to predict ionization–excitation cross sections for electron impact on helium. In this section, a short description of these methods is given. Further details about these calculations are given elsewhere (Bartschat and Grum-Grzhimailo 2002).

We performed calculations for electron-impact ionization–excitation of He(1s<sup>2</sup>) leading to the final ionic state He<sup>+</sup>(2p). We used the computer code RMATRIX-ION of Bartschat (1993), which is based on the formalism outlined by Bartschat and Burke (1987). For some of the higher incident energies, we approximately accounted for second-order effects through the method described in detail by Reid *et al* (1998, 2000). Briefly, the physical idea behind these

hybrid models is to describe the interaction of a ‘fast’ projectile with the initial target bound state and the final ejected-electron–residual-ion system perturbatively to first and, if possible, to second order. Furthermore, the initial bound state and the ejected-electron–residual-ion system alone are described by a convergent ‘*R*-matrix with pseudo-states’ (RMPS) model, in which a large number of physical bound as well as pseudo bound and continuum states are coupled to achieve sufficiently converged results for the parameters of interest for the ejected-electron–residual-ion interaction, most importantly the initial bound state representation and the excitation cross sections for e<sup>−</sup>–He<sup>+</sup> collisions. Note that exchange effects between the fast projectile and the target are neglected.

While the above model is well defined, particularly at the first-order level (DWB1+RMPS), and can be used to provide benchmarks for further studies (see, for example, Kheifets *et al* 1999), the first-order model is well known to be inadequate for the ionization–excitation problem, even for incident energies of several hundred electronvolts. The principal reason for the failure of this model is the fact that the first-order result for the ionization–excitation process is exactly zero if electron–electron correlations are neglected (Marchalant *et al* 1998). Although non-zero cross sections are usually predicted in sophisticated calculations through the use of a highly correlated initial bound state, the above result nevertheless suggests that second-order effects between the projectile and the target may be very important as well. Indeed, this importance was demonstrated in several recent publications (Marchalant *et al* 1998, 1999, Fang and Bartschat 2001a, 2001b, 2001c, Bartschat and Grum-Grzhimailo 2002). Of interest for what follows might be the fact that the double-differential cross section predicted by Bartschat and Grum-Grzhimailo (2002) for an incident electron energy of 200 eV and an ejected-electron energy of 1.2 eV (without observation of the slow electron) was predicted to be substantially larger in the second-order (DWB2 + RMPS) than in the first-order model. Unfortunately, there are several difficulties associated with the above model, particularly when it comes to the calculation of total cross sections, integrated over the angular and energy distributions of both outgoing electrons. Already in first order, the neglect of exchange effects becomes problematic when the continuum electrons in the final state have comparable energies. In practice, however, this may not be too critical if the dominant contributions to the cross sections originate from situations where the energy is shared very asymmetrically between these electrons. This can be expected if the incident energy is sufficiently high, several times the threshold for the simultaneous ionization–excitation process.

Furthermore, the problems associated with the approximations made in evaluating the second-order contribution (see Reid *et al* (1998, 2000) for details) are more significant in the case of integral than for double-differential or triple-differential cross sections. In particular, we found a strong sensitivity of the second-order results on the average energy used to evaluate the second-order term through a closure-type approximation. The results presented in figure 3 (see section 4.2 below), therefore, have to be taken with great care. Tests performed by varying the average energy ‘within reason’, i.e. somewhere between the initial and the final energy of the projectile, showed a sensitivity of about  $\pm 20\%$  for the lowest energy (220 eV,  $v = 4$  au) shown. As expected, that sensitivity slowly decreases with increasing incident energy, but it grows dramatically for lower energies, thereby making more reliable DWB2 + RMPS predictions currently impossible.

#### 4. Results and discussion

Our EUV measured polarization fractions, total and magnetic sublevel cross sections, together with their ratios for the investigated projectiles in this study, are summarized in tables 1–3, where the estimated uncertainties are also given and displayed in figures 1–5.

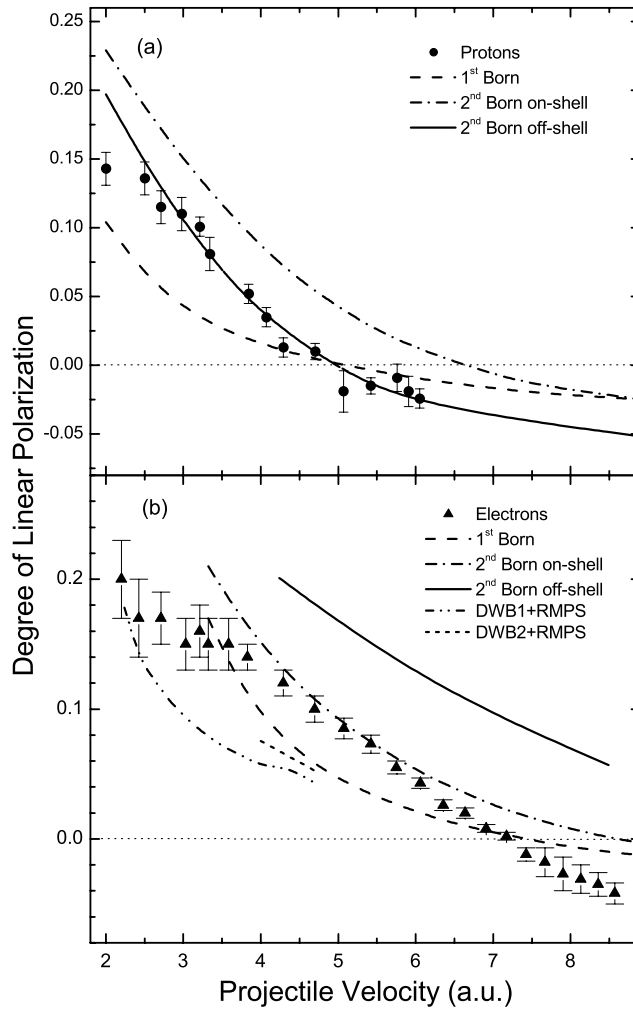


**Figure 1.** Polarization of  $\text{He II}(2p)^2P^0 \rightarrow (1s)^2S$  radiation as a function of electron and proton velocity compared with 1st, 2nd Born calculations. Also shown are hybrid first-order DWB1 + RMPS and second-order DWB2 + RMPS predictions for electron impact.

#### 4.1. Degree of linear polarization

The measured polarization fractions, for electron and proton impact, are depicted in figure 1 along with our previous first- and second-Born (Godunov *et al* 2001, Merabet *et al* 2002b) as well as our DWB1 + RMPS and DWB2 + RMPS predictions. We note here that second-Born on-shell includes only spatial correlation while the full second-Born calculations (second-Born off-shell) account for both spatial and temporal correlations. Figure 1(a) exhibits an excellent convergence of the full second-Born calculations towards the experimental data for proton impact. However, this is not the case for electron impact, where the second-Born off-shell results fail to reproduce our polarization measurements. It is evident from figure 1(b) that the second-Born on-shell results match the EUV polarization fraction in most of the investigated velocity range, whereas the off-shell second-Born predictions are found to be much higher than experimental data. The electron-impact second-Born calculations are more sensitive to

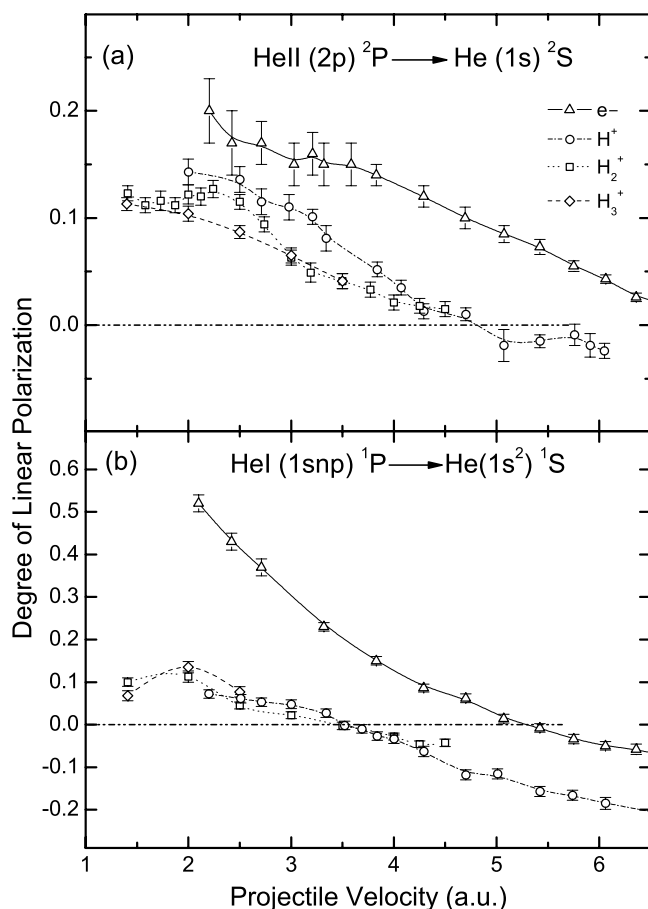


**Figure 2.** Degree of linear polarization of He I and He II EUV radiations as a function of projectile velocity for electron, proton, and molecular hydrogen ( $\text{H}_2^+$  and  $\text{H}_3^+$ ) impact. The lines are provided to guide the eyes. Notations in (b) are the same as in (a).

the quality and number of the intermediate states and this may explain such deviations from experiment. Overall, none of the theoretical methods matches the experimental results for electron impact in a satisfactory way.

Figure 2 shows the He II( $2p$ )<sup>2</sup>P degree of linear polarization measurements for electron, proton, and molecular hydrogen ( $\text{H}_2^+$  and  $\text{H}_3^+$ ) impact velocities. The He I( $1snp$ )<sup>1</sup>P polarization fractions are also included in the lower part of this figure for comparison. In fact, it is interesting to compare these He I results with He II( $2p$ ) measurements in order to clarify diverse collision processes. As can be seen in figure 2, the He I degree of linear polarization following positively charged projectile impact on helium has the same trend while, for electrons, it exhibits a distinct velocity dependence. In particular, the polarization fraction is zero for protons at the same  $\text{H}_2^+$  impact velocity and shows almost identical values for  $\text{H}_2^+$  and  $\text{H}_3^+$  in the 1.4–2.5 au velocity range. In figure 2(a), we can still distinguish between polarization results as function of electron and proton velocities, but their values are much closer than in He I, especially at lower impact energies, exhibiting a visibly different velocity dependence. Moreover, molecular hydrogen polarization fractions for He II seem to be quite

**Table 1.** Experimental data for total  $\sigma$  and magnetic sublevel  $\sigma_0$  and  $\sigma_1$  cross sections, degree of linear polarization, and cross section ratios of  $\sigma_0/\sigma_1$  for ionization–excitation of helium to He II(2p)<sup>2</sup>P<sup>o</sup> following electron impact. The cross sections are given in units of 10<sup>−20</sup> cm<sup>2</sup>. (Notes:  $E$  is the electron energy;  $v$  is the electron velocity.)

$E$ (eV)	$v$ (au)	$P$	$\sigma$	$\sigma_0$	$\sigma_1$	$\sigma_0/\sigma_1$
80	2.4	0.17 ± 0.030	2.4 ± 0.2	1.4 ± 0.1	0.50 ± 0.03	2.69 ± 0.49
100	2.7	0.17 ± 0.020	9.3 ± 0.7	5.3 ± 0.4	2.0 ± 0.1	2.69 ± 0.33
140	3.2	0.16 ± 0.020	18.2 ± 1.4	10.2 ± 0.8	4.0 ± 0.2	2.53 ± 0.31
200	3.8	0.14 ± 0.010	20.4 ± 1.5	10.8 ± 1.3	4.8 ± 0.2	2.25 ± 0.13
276	4.5	0.11 ± 0.010	19.4 ± 1.5	9.4 ± 1.1	5.0 ± 0.2	1.89 ± 0.11
340	5.0	0.088 ± 0.009	16.1 ± 1.2	7.3 ± 0.9	4.4 ± 0.2	1.66 ± 0.09
412	5.5	0.067 ± 0.006	12.9 ± 1.0	5.5 ± 0.7	3.7 ± 0.2	1.48 ± 0.05
500	6.1	0.043 ± 0.004	11.6 ± 0.9	4.6 ± 0.6	3.5 ± 0.2	1.29 ± 0.03
575	6.5	0.023 ± 0.004	11.0 ± 0.8	4.0 ± 0.6	3.5 ± 0.2	1.15 ± 0.03
667	7.0	0.006 ± 0.003	8.8 ± 0.7	3.0 ± 0.4	2.9 ± 0.2	1.04 ± 0.02
735	7.3	−0.007 ± 0.008	7.4 ± 0.6	2.4 ± 0.3	2.5 ± 0.2	0.96 ± 0.05
836	7.8	−0.024 ± 0.012	5.8 ± 0.4	1.8 ± 0.2	2.0 ± 0.1	0.86 ± 0.06
980	8.5	−0.039 ± 0.009	5.3 ± 0.4	1.5 ± 0.2	1.9 ± 0.1	0.79 ± 0.05

**Table 2.** Experimental data for total  $\sigma$  and magnetic sublevel  $\sigma_0$  and  $\sigma_1$  cross sections, degree of linear polarization, and cross section ratios of  $\sigma_0/\sigma_1$  for ionization–excitation of helium to He II(2p)<sup>2</sup>P<sup>o</sup> following proton impact. The cross sections are given in units of 10<sup>−20</sup> cm<sup>2</sup>. (Notes:  $E$  is the proton energy;  $v$  is the proton velocity.)

$E$ (keV)	$v$ (au)	$P$	$\sigma$	$\sigma_0$	$\sigma_1$	$\sigma_0/\sigma_1$
100	2.0	0.143 ± 0.012	101.8 ± 12.5	54.4 ± 8.7	23.7 ± 3.8	2.29 ± 0.16
156	2.5	0.136 ± 0.012	55.4 ± 6.9	29.0 ± 4.7	13.2 ± 2.1	2.20 ± 0.15
225	3.0	0.105 ± 0.012	29.1 ± 3.6	13.9 ± 2.2	7.6 ± 1.2	1.83 ± 0.13
307	3.5	0.073 ± 0.008	19.0 ± 2.5	8.2 ± 1.3	5.4 ± 0.8	1.53 ± 0.07
368	3.8	0.05 ± 0.007	19.7 ± 2.7	7.9 ± 1.2	5.9 ± 0.9	1.34 ± 0.05
400	4.0	0.039 ± 0.007	14.0 ± 1.9	5.4 ± 0.8	4.3 ± 0.7	1.26 ± 0.05
626	5.0	−0.005 ± 0.013	9.2 ± 1.2	3.0 ± 0.5	3.1 ± 0.5	0.97 ± 0.08
916	6.1	−0.024 ± 0.008	5.7 ± 0.8	1.7 ± 0.2	2.0 ± 0.3	0.86 ± 0.04

**Table 3.** Experimental data for total  $\sigma$  and magnetic sublevel  $\sigma_0$  and  $\sigma_1$  cross sections, degree of linear polarization, and cross section ratios of  $\sigma_0/\sigma_1$  for ionization–excitation of helium to He II(2p)<sup>2</sup>P<sup>o</sup> following hydrogen molecular (H<sub>2</sub><sup>+</sup> and H<sub>3</sub><sup>+</sup>) impact. The cross sections are given in units of 10<sup>−20</sup> cm<sup>2</sup>. (Notes:  $E$  is the projectile energy;  $v$  is the projectile velocity.)

Projectile	$E$ (keV)	$v$ (au)	$P$	$\sigma$	$\sigma_0$	$\sigma_1$	$\sigma_0/\sigma_1$
H <sub>2</sub> <sup>+</sup>	100	1.4	0.123 ± 0.007	233.7 ± 34.8	117.7 ± 17.6	58.0 ± 7.5	2.04 ± 0.08
	200	2	0.122 ± 0.009	151.9 ± 22.9	76.5 ± 11.5	37.7 ± 4.7	2.02 ± 0.11
	312	2.5	0.115 ± 0.007	93.7 ± 14.2	46.1 ± 13.0	23.8 ± 3.1	1.94 ± 0.08
	450	3	0.063 ± 0.007	56.8 ± 8.7	23.8 ± 7.0	16.5 ± 2.2	1.44 ± 0.06
	612	3.5	0.041 ± 0.007	32.6 ± 4.9	12.8 ± 1.9	9.9 ± 1.3	1.27 ± 0.05
	800	4	0.021 ± 0.007	31.8 ± 4.6	11.6 ± 1.7	10.1 ± 1.4	1.13 ± 0.05
H <sub>3</sub> <sup>+</sup>	150	1.4	0.113 ± 0.006	110.4 ± 16.8	54.2 ± 8.1	28.1 ± 3.8	1.92 ± 0.07
	300	2	0.104 ± 0.007	220.9 ± 33.0	105.5 ± 15.8	57.7 ± 7.6	1.82 ± 0.07
	468	2.5	0.087 ± 0.006	177.1 ± 26.7	80.3 ± 12.0	48.4 ± 6.6	1.65 ± 0.06
	674	3	0.065 ± 0.007	82.4 ± 12.5	34.8 ± 5.1	23.8 ± 3.2	1.46 ± 0.06
	918	3.5	0.041 ± 0.007	72.7 ± 11.0	28.1 ± 4.2	22.3 ± 3.0	1.27 ± 0.05

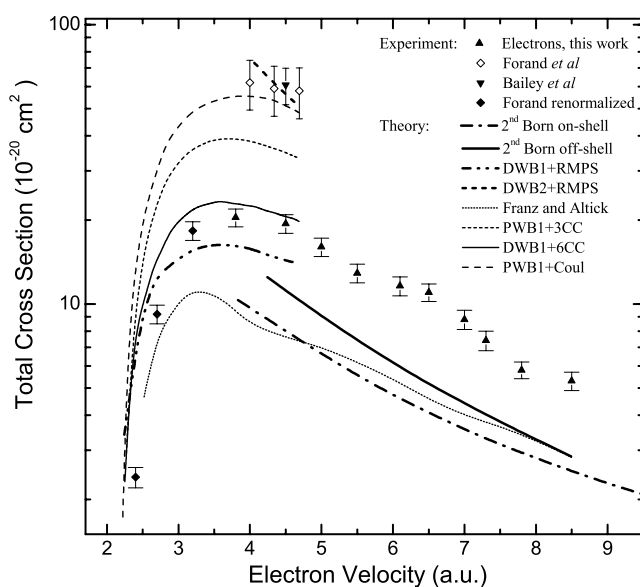


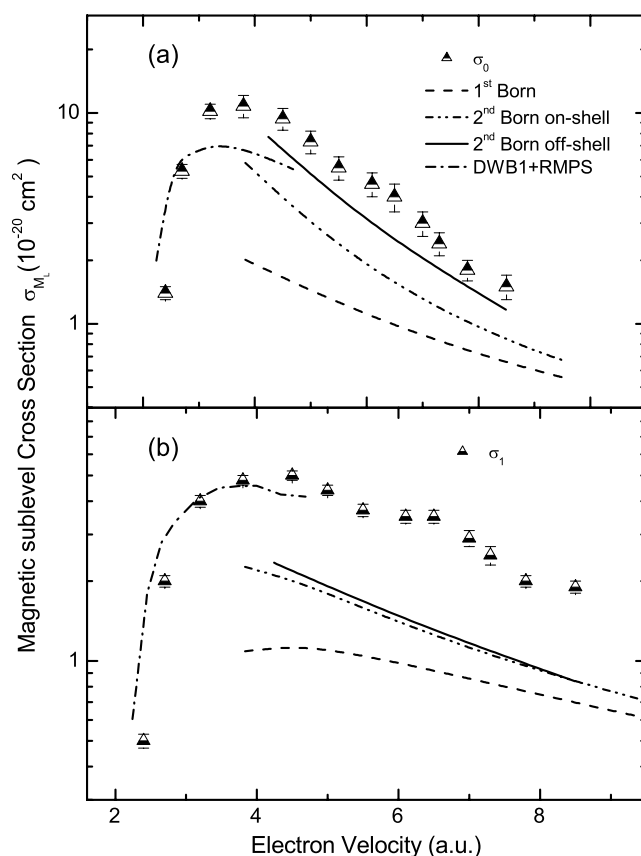
**Figure 3.** Total cross sections for ionization–excitation to He II(2p)<sup>2</sup>P<sup>0</sup> states as a function of electron velocity, compared with various theoretical predictions.

different from those of protons within the velocity range investigated. Such distinction is found to be further pronounced for H<sub>3</sub><sup>+</sup> projectiles. On the other hand, the H<sub>2</sub><sup>+</sup> data show a minimum at 1.5 au, followed by a gradual increase and then decrease as a function of the velocity while the H<sub>3</sub><sup>+</sup> results have a constant decline. Since a more refined theoretical description of such complex multi-centre collision processes does not currently exist, little can be said about contributions to the total scattering amplitude due to multi-centre scattering and interference effects in such complex collision systems. Nevertheless, comparison of the velocity dependence corresponding to the polarization fraction for He I and He II measurements indicates that, for the excitation process, H<sub>2</sub><sup>+</sup> and H<sub>3</sub><sup>+</sup> projectiles act on helium like two and three independent protons, respectively. For the ionization–excitation mechanism, on the other hand, our EUV results suggest that the electron–electron interaction should be accounted for, because the polarization and therefore the angular distributions are not just sensitive to the projectile charge but also to its mass and structural complexity.

#### 4.2. Total and magnetic sublevel cross sections

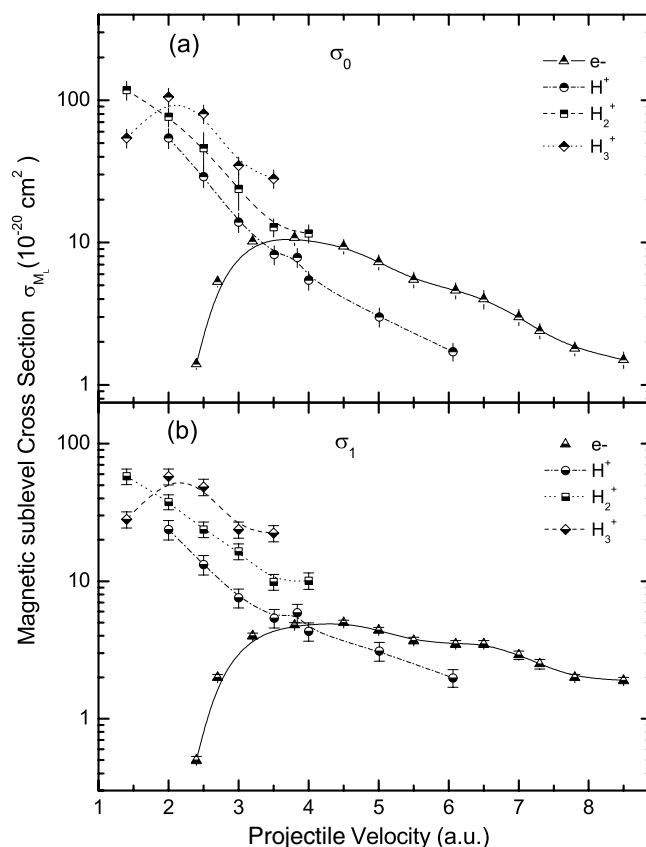
Using equations (3) and (4), we have derived the scattering-angle-integrated magnetic sublevel cross sections,  $\sigma_0$  and  $\sigma_1$  for  $M_L = 0, \pm 1$ , associated with the excited states He II(2p)<sup>2</sup>P<sup>0</sup> following He<sup>+</sup>(2p)<sup>2</sup>P<sup>0</sup> → (1s)<sup>2</sup>S transition ( $\lambda = 30.4$  nm) in e<sup>-</sup> + He and H<sub>*m*</sub><sup>+</sup> + He ( $m = 1-3$ ) collisions at impact energies ranging from 80 to 980 eV ( $2.4 < v_{e^-} < 8.5$  au), 100 to 916 keV ( $2 < v_{H^+} < 6$  au), 100 to 800 keV ( $1.4 < v_{H_2^+} < 4$  au), and 150 to 918 keV ( $1.4 < v_{H_3^+} < 3.5$  au), respectively.

Figure 3 exhibits the observed He<sup>+</sup>(2p)<sup>2</sup>P<sup>0</sup> total cross sections compared with our recent predictions as well as other theoretical calculations for electrons. In particular, we show in this figure earlier theoretical total cross sections for electron impact on helium; namely, second-Born results of Franz and Altick (1985), the hybrid plane-wave plus three-state model (PWB1 + 3CC) of Rudge (1988), the six-state (DWB1 + 6CC) model of



**Figure 4.** Magnetic sublevel scattering-angle-integrated cross sections  $\sigma_0$  (a) and  $\sigma_1$  (b) for excitation to He II(2p)<sup>2</sup>P<sup>0</sup> states as a function of electron velocity compared with corresponding theoretical predictions. Notations in (b) are the same as in (a) unless indicated otherwise.

Raeker *et al* (1994), and the Coulomb–Born results (PWB1 + Coul) of Kuplyauskene and Maknitskas (1991). These are compared with the experimental data of Bailey *et al* (1995) and our EUV renormalized (see Merabet *et al* (2002b), for details regarding this renormalization) measurements, the original data of Forand *et al* (1985) for  $4 < v < 4.7$  au and the renormalized ones for the three lower velocity impact ( $2.4 < v < 3$ ), our recent second-Born calculations, as well as our present DWB1 + RMPS and DWB2 + RMPS predictions. Although the 6-state results of Raeker *et al* (1994) seem to be in excellent agreement with our measurements in the 3–5 au velocity range, this agreement is likely accidental since improving the model actually decreases the predicted cross sections, resulting in poorer agreement with experiment. Note that the predicted cross sections in these models go down when the descriptions of the initial state and the ejected-electron–residual-ion interaction are improved, as can be seen by comparing the numbers from Coulomb–Born results (PWB1 + Coul), the three-state model (PWB1 + 3CC), the six-state model (DWB1 + 6CC), and the present DWB1 + RMPS calculations (figure 3). Also shown in figure 3 are a few results from our second-order calculations (DWB2 + RMPS). As mentioned in section 3, however, these numbers have to be taken as with great care, because of the multitude of physical and numerical approximations. Nonetheless, it is interesting that the predicted values are about a factor of five larger than the first-order numbers, in qualitative agreement with the original measurements of Forand *et al* (1985) and of Bailey *et al* (1995).



**Figure 5.** Experimental sublevel cross sections  $\sigma_0$  (a) and  $\sigma_1$  (b) as a function of projectile velocities compared for electron, proton, and molecular hydrogen ( $H_2^+$  and  $H_3^+$ ) impact. Curves are provided to guide the eye.

The total cross sections predicted by Franz and Altick are consistent with our full second-Born results at the high impact energies. We note that neither second-Born on-shell nor second-Born off-shell results converge to the experimental cross sections for electron projectiles. Nevertheless, the difference between our full second-Born results and experiment is less than the factor 3 deviation between the pioneering calculations of Franz and Altick (1985) and previous measurements (Forand *et al* 1985).

The sublevel cross sections  $\sigma_0$  and  $\sigma_1$  for He II(2p)<sup>2</sup>P<sup>o</sup> states for electron impact are depicted in figure 4 and compared with our present DWB1 + RMPS as well as on-shell and off-shell Born calculations for impact velocities  $v \geq 3.8$  au since at lower energies higher-order terms beyond second-order are expected to be significant (Godunov *et al* 2001). The behaviour of the  $\sigma_0$  and  $\sigma_{\pm 1}$  cross sections is qualitatively similar to the total cross section for excitation–ionization. The first-Born cross sections and experimental data do not converge in the investigated velocity range. The second-Born effect including off-shell terms increases the first-Born cross sections and therefore improves agreement with the EUV measurements. Such convergence is good for  $\sigma_0$  but still not satisfactory for  $\sigma_{\pm 1}$ . Once again, the persistent disagreement between theory and experiment emphasizes the need for even more sophisticated calculations.

As a further investigation of the ionization–excitation process for positively and negatively singly charged projectiles, we have examined the dependence of sublevel cross sections for different projectile impacts. Figure 5 exhibits such a comparison of these observables. The general trend for the measured sublevel cross sections following electron impact shows a steep increase in cross section for small impact velocities, reaching a maximum around 4 au. Then follows a gradual decrease with increasing electron velocity towards the asymptotic high-energy limit. However, significant differences between electron, proton, and molecular hydrogen impact occur over the whole investigated velocity range. Specifically, it is observed that the sublevel cross sections for the positively charged ion impact are larger than those obtained for electron impact at lower velocities ( $v < 3.5$  au). Then they continue to decrease as the impact velocity increases and become smaller than the electron cross sections at higher ion energies. Furthermore (see also the polarization data), the  $\sigma_0$  cross sections are found to be bigger than the  $\sigma_1$  results on the entire investigated energy range. In addition, the sublevel cross sections exhibit distinct velocity dependence for  $H_3^+$  ions when compared with  $H_2^+$  impact results. Indeed, cross sections for  $H_2^+$  results show a continuous decline as a function of the projectile velocity impact while the  $H_3^+$  sublevel cross sections show a maximum at  $v_{H_3^+} = 2.0$  au. To our knowledge, there is no theory for the simultaneous ionization–excitation mechanism involved in molecular hydrogen ion impact on helium. The results in the present experimental database may therefore serve as benchmarks to test future theoretical calculations on such complex collision systems.

## 5. Summary and conclusions

We have presented a rigorous compilation of experimental and theoretical EUV spectro-polarimetric data. In particular, we have reported the first polarization measurements following ionization–excitation of helium by molecular hydrogen ions ( $H_2^+$  and  $H_3^+$ ) for impact velocities ranging from 1.4 to 4.0 and 1.4 to 3.5 au, respectively. The degree of linear polarization measurements are compared for different projectiles ( $e^-$ ,  $H^+$ ,  $H_2^+$  and  $H_3^+$ ) as function of their impact velocities following both excitation and simultaneous ionization–excitation processes. Measured angle-integrated sublevel cross sections are presented for all the above projectiles colliding with helium, and a detailed comparison of the experimental data for electrons and protons with previous and recent first- and second-order advanced theoretical approaches is given in order to elucidate the mechanisms involved during the collision.

Furthermore, based upon excellent agreement between theory and experiment for the polarization fractions determined under identical experimental conditions for proton impact on helium, we have proposed new normalized total cross sections that may overcome the factor 2 or 3 deviation between various theoretical predictions and previous electron-impact measurements. Only modest agreement is found between our theoretical results and the experimental data for electron impact, suggesting the need for more sophisticated treatments of the target description and/or the inclusion of higher-order terms. Nevertheless, these findings lend support to the new normalization procedure suggested by Merabet *et al* (2002b) since agreement is nearly reached between experiment and theory for  $e^- + He$  and  $H^+ + He$  scattering. However, a final conclusion on this matter may need additional measurements with better EUV filters than those used by Forand *et al* (1985).

## Acknowledgments

We would like to thank Dr Grum-Grzhimailo from Moscow State University for his interesting and fruitful suggestions. This project was supported in part by the Nevada Business and

Science Foundation (NBSF), Reno, Nevada and Applied Photonics Worldwide (APW) Inc. KB acknowledges support from the National Science Foundation under grant PHY-0244470.

## References

- Bailey M, Bruch R, Rauscher E and Bliman S 1995 *J. Phys. B: At. Mol. Opt. Phys.* **28** 2655
- Bailey M, Merabet H and Bruch R F 1999 *Appl. Opt.* **38** 4125
- Balashov V V and Bodrenko I V 1999 *J. Phys. B: At. Mol. Opt. Phys.* **32** L687
- Bartschat K 1993 *Comput. Phys. Commun.* **75** 219
- Bartschat K and Burke P G 1987 *J. Phys. B: At. Mol. Phys.* **20** 3191
- Bartschat K and Grum-Grzhimailo A N 2002 *J. Phys. B: At. Mol. Opt. Phys.* **35** 5035
- Bruch R, Beigman I L, Rauscher E A, Fülling S, McGuire J H, Träbert E and Heckmann P H 1993 *J. Phys. B: At. Mol. Opt. Phys.* **26** L143
- Bruch R, Wang H, Godunov A L, Ivanov P B, Schipakov V A and Merabet H 2002 *J. Phys. B: At. Mol. Opt. Phys.* **35** 1
- Dogan M, Crowe A, Bartschat K and Marchalant P J 1998 *J. Phys. B: At. Mol. Opt. Phys.* **31** 1611 and references therein
- Fang Y and Bartschat K 2001a *J. Phys. B: At. Mol. Opt. Phys.* **34** L19
- Fang Y and Bartschat K 2001b *J. Phys. B: At. Mol. Opt. Phys.* **34** 2747
- Fang Y and Bartschat K 2001c *Phys. Rev. A* **64** 020701(R)
- Forand J L, Becker K and McConkey J W 1985 *J. Phys. B: At. Mol. Phys.* **18** 1409
- Franz A and Altick P L 1985 *J. Phys. B: At. Mol. Phys.* **28** 4639
- Fülling S, Bruch R, Rauscher E A and Neil P 1992 *Phys. Rev. Lett.* **68** 3152
- Godunov A L, McGuire J H, Ivano P B, Shipakov V A, Merabet H, Bruch R, Hanni J and Shakov K K 2001 *J. Phys. B: At. Mol. Opt. Phys.* **34** 5055
- Götz A, Mehlhorn W, Raeker A and Bartschat K 1996 *J. Phys. B: At. Mol. Opt. Phys.* **29** 4699
- Haidt D and Kleinpoppen H 1966 *Z. Phys.* **190** 72
- Hayes P A and Williams J F 1996 *Phys. Rev. Lett.* **77** 3098
- Heddl D W O and Gallagher J W 1989 *Rev. Mod. Phys.* **61** 221
- Kheifets A, Bray I and Bartschat K 1999 *J. Phys. B: At. Mol. Opt. Phys.* **32** L433
- Kuplyauskene A V and Maknitskas A A 1991 *Opt. Spectrosc.* **71** 127
- Marchalant P J, Rasch J, Whelan C T, Madison D H and Walters H R J 1999 *J. Phys. B: At. Mol. Opt. Phys.* **32** L705
- Marchalant P J, Whelan C T and Walters H R J 1998 *J. Phys. B: At. Mol. Opt. Phys.* **31** 1141
- McConkey J W, Hammond P and Khakoo M A 1988 *Electronic and Atomic Collisions* ed H B Gilbody *et al* (Amsterdam: Elsevier) p 105
- McGuire J H 1997 *Electron Correlation Dynamics in Atomic Collisions* (Cambridge: Cambridge University Press)
- Merabet H, Bailey M, Bruch R, Fursa D V, Bray I, McConkey J W and Hammond P 1999 *Phys. Rev. A* **60** 1187
- Merabet H, Bailey M, Bruch R, Hanni J, Bliman S, Fursa D V, Bray I, Bartschat K, Tseng H C and Lin C D 2001a *Phys. Rev. A* **64** 12712
- Merabet H, Bruch R, Bailey M, Hanni J, Fineschi S, Godunov A, McGuire J H, Bray I, Bartschat K, Tseng H C and Lin C D 2001b *Proc. SPIE* **4498** 207
- Merabet H, Bruch R, Fülling S, Bartschat K, Godunov A L, McGuire J H and Grum-Grzhimailo A N 2002a *Proc. SPIE* **4819** 118
- Merabet H, Bruch R, Hanni J, Godunov A L and McGuire J H 2002b *Phys. Rev. A* **65** R010703
- Niehaus A 1986 *J. Phys. B: At. Mol. Phys.* **19** 2925
- Percival I C and Seaton M J 1958 *Phil. Trans. R. Soc. A* **251** 113
- Raeker A, Bartschat K and Reid R H G 1994 *J. Phys. B: At. Mol. Opt. Phys.* **27** 3129
- Reid R H G, Bartschat K and Raeker A 1998 *J. Phys. B: At. Mol. Opt. Phys.* **31** 563
- Reid R H G, Bartschat K and Raeker A 2000 *J. Phys. B: At. Mol. Opt. Phys.* **33** 5261 (corrigendum)
- Rouvellou B, Rioual S, Pachat A, Tweed R J, Langlois J, Vien Nguyen G and Robaux O 2000 *J. Phys. B: At. Mol. Opt. Phys.* **33** L599
- Rudge M R H 1988 *J. Phys. B: At. Mol. Opt. Phys.* **21** 1887
- Stolte W and Bruch R 1996 *Phys. Rev. A* **54** 2166